Electronic Supplementary Information

The Unsuspected Influence of the Pyridyl-Triazole Ligand Isomerism upon the Electronic Properties of Tricarbonyl Rhenium Complexes: An Experimental and Theoretical Insight

Jinhui Wang, Béatrice Delavaux-Nicot, Mariusz Wolff, Sonia Mallet-Ladeira, Rémi Métivier, Eric Benoist and Suzanne Fery-Forgues

List of Tables

Table S1. Crystallographic data and structure refinement details for **ReL1** and **ReL2**..... 3

Table S2. Selected hydrogen bonding distances (Å) and angles (°) and comments on hydrogen bonding……..……... 4

Table S3. Experimental and theoretical selected bond lengths and angles for **ReL1** 6

Table S4. Experimental and theoretical selected bond lengths and angles for **ReL2**..... 7

Table S5. Atomic charges from the Natural Population Analysis (NPA) 8

Table S6. Occupancy and hybridization of the calculated natural bond orbitals (NBOs) between the rhenium and the carbonyl ligands for **ReL1** and **ReL2**…… 8

Table S7. Natural populations of the 5*d* orbitals of the central atom in **ReL1** and **ReL2**…. 9

Table S8. Absolute electronegativity, absolute hardness, dipole moment, electrophilicity index and global softness of complexes **ReL1** and **ReL2**……. 9

Table S9. Energy levels and composition of selected frontier molecular orbitals for complexes **ReL1** and **ReL2** in CH_2Cl_2……... 9

Table S10. Main electronic transitions for **ReL1** calculated with TD-DFT method …..… 10

Table S11. Main electronic transitions for **ReL2** calculated with TD-DFT method …….. 10

Table S12. Four calculated lowest singlet excited states for **ReL1** and **ReL2** in S_1 optimized geometry ..…….. 11

Table S13. Calculated phosphorescence emission energies of **ReL1** and **ReL2** …… 11

Table S14. Experimental electrochemical data and calculated values of the energy gaps (E_g) for **ReL1** and **ReL2**. Comments on the evaluation of E_g for the Re complexes ……. 11

Table S15. Full spectroscopic data in three organic solvents ……. 12

Table S16. Results of the emission decay measurements of the complexes in the solid state ……..... 12

Table S17. Cartesian coordinates of complex **ReL1** …….. 13

Table S18. Cartesian coordinates of complex **ReL2** …….. 14

List of Figures

Figure S1. Hydrogen bonding and distances between centroids in **ReL1** ……... 15

Figure S2. Hydrogen bonding and distances between centroids in **ReL2** ……... 16

Figure S3. Molecular electrostatic potential (MEP) surface of **ReL1** and **ReL2**…….. 17

Figure S4. OSWV study. Anodic and cathodic scans of ligand **L1** and **L2** 18

Figure S5. Cyclic voltammograms of ligands **L1** and **L2** at 0.2 V/s..…….. 18

Figure S6. First reduction process of complex **ReL1** at different scan rates.……... 18

Figure S7. Cyclic voltammograms of complexes **ReL1** and **ReL2** at 0.2 V/s.…… 19

Figure S8. Cyclic voltammograms of **ReL1** on a glassy carbon working electrode at 0.2 V/s ……. 19

Figure S9. Experimental *vs.* simulated UV-vis absorption spectra of **ReL1** and **ReL2**……. 19

Figure S10. Fluorescence decays of complexes **ReL1** and **ReL2** in dichloromethane ……. 20

Figure S11. Fluorescence decays of complexes **ReL1** and **ReL2** in the solid state (powder) ..……..... 20

Figure S12. Proton numbering scheme for NMR …… 21

TABLES

Table S1. Crystallographic data and structure refinement details for **ReL1** and **ReL2**.

	ReL1	**ReL2**
Empirical formula	$2(C_{23}H_{13}ClN_5O_4Re).C_2H_3N$	$C_{23}H_{13}ClN_5O_4Re.C_3H_6O$
Formula weight	1331.14	703.12
Temperature [K]	193.0(2)	193.0(2)
Wavelength [Å]	0.71073	0.71073
Crystal system	Monoclinic	Monoclinic
Space group	$P2_1/n$	$P2_1/c$
Unit cell dimensions [Å,°]	a = 17.9665(7)	a = 6.6979(5)
	b = 11.6047(4)	b = 19.6258(13)
	c = 25.2810(9)	c = 19.4187(13)
	β = 104.804(2)	β = 91.552(3)
Volume [Å3]	5096.0(3)	2551.7(3)
Z	4	4
Density (calculated) [Mg/m^3]	1.735	1.830
Absorption coefficient [mm^{-1}]	4.914	4.914
F(000)	2568	1368
Crystal size [mm]	0.12 × 0.04 × 0.04	0.38 × 0.02 × 0.02
θ range for data collection [°]	4.15 to 25.35	3.65 to 25.02
Index ranges	$-21 \le h \le 21$ $-13 \le k \le 13$ $-30 \le l \le 30$	$-7 \le h \le 7$ $-23 \le k \le 23$ $-21 \le l \le 23$
Reflections collected	129739	28067
Independent reflections	9290 [R(int) = 0.0735]	4484 [R(int) = 0.0731]
Completeness to 2theta = (°)	(25.35°) 99.5 %	(25.02°) 99.6 %
Min. and max. transm.	0.7461 and 0.6305	0.7457 and 0.6129
Data / restraints / parameters	9290 / 394 / 757	4484 / 0 / 345
Goodness-of-fit on F2	1.059	1.029
Final R indices [$I>2\sigma(I)$]	R1 = 0.0355 wR2 = 0.0849	R1 = 0.0354 wR2 = 0.0612
R indices (all data)	R1 = 0.0531 wR2 = 0.0932	R1 = 0.0613 wR2 = 0.0681
Largest diff. peak and hole [e $Å^{-3}$]	1.792 and -1.108	0.666 and -0.868
CCDC	CCDC 1555800	CCDC 1555801

Table S2. Selected hydrogen bonding distances (Å) and angles (°) of **ReL1** and **ReL2**.

D	**A**	**D—H** [Å]	**H···A** [Å]	**D···A** [Å]	**D—H···A** [°]
			ReL1		
C(5)—H(5)···O(1)_#1		0.95	2.56	3.359(8)	141.9
C(10)—H(10)···Cl(1)_#2		0.95	2.67	3.550(7)	154.6
C(12)—H(12)···O(5)		0.95	2.44	3.306(8)	151.2
C(15)—H(15)···O(6)_#3		0.95	2.47	3.186(9)	131.8
C(24)—H(24)···O(4)		0.95	2.48	2.804(9)	99.8
C(44)_a—H(44)_a···O(8)_a		0.95	2.45	2.797(13)	101.1
			ReL2		
C(7)—H(7)···O(5)		0.95	2.57	3.482(9)	160.6
C(10)—H(10)···O(5)		0.95	2.07	2.987(8)	160.4
C(19)—H(19)···O(3)_#4		0.95	2.60	3.545(8)	174.5
C(23)—H(23)···O(4)		0.95	2.46	2.797(7)	100.6

Symmetry codes: #1: 3/2–x, 1/2+y, 3/2–z; #2: 1–x, –y, 1–z; #3: x, –1+y, z; #4: 1+x, 1/2–y, –1/2+z; #5: 1–x, –y, 1–z.

Comments on hydrogen bonding.

The selected hydrogen bonding distances and angles of **ReL1** and **ReL2** are shown in Table S2. Complex **ReL1** crystallizes with two crystallographically independent molecules of [Re(CO)$_3$(**L1**)Cl] and one non-coordinating acetonitrile molecule in the asymmetric unit.
The crystal structure of **ReL1** is stabilized by a network of classical intermolecular hydrogen bonding interactions. Three interactions are of the type C—H···O between 2-C(5)–H proton of the 2-pyridyl group and carbonyl oxygen O(1), C(12)–H proton of the benzoxazole and carbonyl oxygen O(5), and C(15)–H proton of the benzoxazole and carbonyl oxygen O(5), and one interaction is of the type C—H···Cl (3.550(7) Å) between C(10)–H proton of triazole and Cl(1) attached to the rhenium atom (Figure S3). Additionally, one intramolecular hydrogen bonding C—H···O interaction between C–H proton of the phenyl ring and the benzoxazole oxygen atom O is also observed in the crystal lattice. Moreover, there are also π–π stacking interactions between two parallel 2-pyridine rings (symmetry code: 3/2–x, 1/2+y, 3/2–z) [with a centroid-to-centroid distance of 4.084(4) Å and an interplanar α angle between the planes of these rings of 5.0(3)°, slipping angles β or γ of 35.03° or 36.95°], two parallel triazole rings (symmetry code: 1–x,1–y,1–z) [with a centroid-to-centroid distance of 3.584(3) Å and an interplanar α angle between the planes of these rings of 0°, slipping angles β or γ of 25.62° or 25.62° and slippage of 1.550 Å], as well as two anti-parallel 2-phenylbenzoxazole moieties of the neighboring complex molecules [centroid-to-centroid distance between the 2-phenyl ring and the oxazole ring of benzoxazole (symmetry code: 2–x, –y,1–z) is equal to 4.425(5) Å, whereas an interplanar α angle between the planes of these rings is 6.1(4)° and slipping angles β or γ are 36.17° or 38.82°, respectively; centroid-to-centroid distance between the 2-phenyl ring and the benzene ring of benzoxazole (symmetry code: 2–x, –y,1–z) is equal to 4.367(5) Å, whereas an interplanar α angle between the planes of these rings is 8.4(4)° and slipping angles β or γ are 41.87° or 34.34°, respectively], that take part in the stabilization of the crystal lattice.

Complex **ReL2** crystallizes with one non-coordinating acetone molecule. The uncoordinated oxygen atom O(5) of the acetone molecule forms two intermolecular hydrogen bonding interactions; stronger with C(10)–H proton of the triazole C—H···O (2.987(8) Å) and weaker with the 5-C(7)–H proton of the 2-pyridyl group C—H···O (3.482(9) Å). Next two intermolecular hydrogen bonding interactions C—H···O between C(19)–H and carbonyl oxygen O(3), as well as between C(21)–H and carbonyl oxygen O(2), also stabilize the crystal structure of **ReL2** (Figure S4). Additionally, one intramolecular hydrogen bonding interaction C—H···O between C(23)–H and the benzoxazole oxygen O(4) is also observed. Slipped π–π stacking interactions between the 2-phenyl ring and the benzene ring of benzoxazole (symmetry code: –1+x, y, z) [with a centroid-to-centroid distance of 3.703(3) Å and an interplanar α angle between the planes of these rings of 7.5(3)°, slipping angles β or γ of 22.31° or 29.41°], the oxazole ring of benzoxazole and the triazole ring (symmetry code: –1+x, y, z) [with a centroid-to-centroid distance of 3.623(3) Å and an interplanar α angle between the planes of these rings of 9.0(3)°, slipping angles β or γ of 23.14° or 14.10°], the benzene ring of benzoxazole and the 2-pyridyl ring (symmetry code: –1+x, y, z) [with a centroid-to-centroid distance of 3.967(3) Å and an interplanar angle α between the planes of these rings of 4.5(3)°, slipping angles β or γ of 30.92° or 29.55°] from adjacent molecules are also present in the crystal structure of complex **ReL2**.

Table S3. Selected experimental and theoretical bond lengths [Å] and angles [°] for **ReL1**. Experimental data are from X-ray analysis; theoretical data have been calculated for molecules with CH_2Cl_2 as solvent medium.

Bond lengths	Experimental	Optimized			Bond angles	Experimental	Optimized		
		S_0	S_1	T_1			S_0	S_1	T_1
Re(1)-C(1)	1.930(8)	1.896	*1.954*	1.951	C(1)-Re(1)-C(2)	90.4(3)	90.35	*93.46*	92.52
Re(1)-C(2)	1.894(8)	1.912	*1.949*	1.933	C(1)-Re(1)-C(3)	91.8(3)	90.60	*90.44*	89.19
Re(1)-C(3)	1.912(7)	1.916	*1.958*	1.986	C(2)-Re(1)-C(3)	88.0(3)	89.69	*85.18*	88.26
Re(1)-N(2)	2.189(5)	2.211	*2.152*	2.165	C(1)-Re(1)-N(2)	95.5(2)	93.83	*88.78*	91.50
Re(1)-N(3)	2.143(5)	2.146	*2.098*	2.041	C(2)-Re(1)-N(2)	171.7(3)	170.82	*173.96*	171.78
Re(1)-Cl(1)	2.4850(17)	2.524	*2.421*	2.455	C(3)-Re(1)-N(2)	97.6(3)	98.43	*100.43*	76.48
					C(1)-Re(1)-N(3)	90.9(2)	94.09	*90.52*	90.68
C(1)-O(1)	1.110(8)	1.164	*1.148*	1.149	C(2)-Re(1)-N(3)	100.5(3)	97.58	*98.20*	96.30
C(2)-O(2)	1.159(9)	1.158	*1.150*	1.153	C(3)-Re(1)-N(3)	171.1(3)	171.31	*176.43*	175.44
C(3)-O(3)	1.150(8)	1.160	*1.151*	1.148	N(3)-Re(1)-N(2)	73.70(19)	73.98	*76.16*	76.48
					C(1)-Re(1)-Cl(1)	176.1(2)	176.43	*174.93*	174.18
					C(2)-Re(1)-Cl(1)	91.4(2)	92.47	*91.56*	91.64
					C(3)-Re(1)-Cl(1)	91.7(2)	91.62	*90.67*	86.87
					N(2)-Re(1)-Cl(1)	82.40(13)	83.07	*86.16*	84.89
					N(3)-Re(1)-Cl(1)	85.35(14)	83.36	*88.07*	92.91
					Re(1)-C(1)-O(1)	175.6(7)	179.84	*179.23*	179.46
					Re(1)-C(2)-O(2)	178.5(7)	178.84	*179.96*	179.03
					Re(1)-C(3)-O(3)	178.8(7)	179.27	*178.58*	179.00
Re(2)-C(25)	1.944(8)				C(27)-Re(2)-C(26)	87.6(3)			
Re(2)-C(26)	1.928(8)				C(27)-Re(2)-C(25)	91.5(3)			
Re(2)-C(27)	1.916(8)				C(26)-Re(2)-C(25)	86.8(3)			
Re(2)-N(7)	2.200(5)				C(27)-Re(2)-N(8)	170.3(3)			
Re(2)-N(8)	2.138(5)				C(26)-Re(2)-N(8)	101.6(2)			
Re(2)-Cl(2)	2.4896(17)				C(25)-Re(2)-N(8)	92.0(2)			
					C(27)-Re(2)-N(7)	96.7(3)			
C(25)-O(5)	1.079(8)				C(26)-Re(2)-N(7)	175.6(2)			
C(26)-O(6)	1.138(8)				C(25)-Re(2)-N(7)	92.3(2)			
C(27)-O(7)	1.151(8)				N(8)-Re(2)-N(7)	74.08(18)			
					C(27)-Re(2)-Cl(2)	93.4(2)			
					C(26)-Re(2)-Cl(2)	95.2(2)			
					C(25)-Re(2)-Cl(2)	174.78(19)			

					N(8)-Re(2)-Cl(2)	82.89(13)			
					N(7)-Re(2)-Cl(2)	85.33(13)			
					Re(2)-C(25)-O(5)	174.6(6)			
					Re(2)-C(26)-O(6)	175.8(6)			
					Re(2)-C(27)-O(7)	179.7(8)			

Table S4. Experimental and theoretical selected bond lengths [Å] and angles [°] for **ReL2.** Experimental data are from X-ray analysis; theoretical data have been calculated for molecules in CH_2Cl_2.

Bond lengths	Experimental	Optimized			Bond angles	Experimental	Optimized		
		S_0	S_1	T_1			S_0	S_1	T_1
Re(1)-C(1)	1.944(7)	1.897	*1.954*	1.950	C(1)-Re(1)-C(2)	90.9(3)	90.44	*93.65*	88.36
Re(1)-C(2)	1.915(6)	1.913	*1.950*	1.990	C(1)-Re(1)-C(3)	88.3(3)	90.55	*90.16*	90.24
Re(1)-C(3)	1.923(7)	1.915	*1.957*	1.929	C(2)-Re(1)-C(3)	90.5(2)	89.57	*85.26*	90.73
Re(1)-N(2)	2.203(4)	2.211	*2.148*	2.079	C(1)-Re(1)-N(2)	94.2(2)	93.66	*88.80*	89.48
Re(1)-N(3)	2.157(4)	2.152	*2.104*	2.130	C(2)-Re(1)-N(2)	169.9(2)	171.24	*173.96*	171.65
Re(1)-Cl(1)	2.4799(17)	2.522	*2.421*	2.451	C(3)-Re(1)-N(2)	98.3(2)	98.13	*176.35*	172.26
					C(1)-Re(1)-N(3)	93.0(2)	94.09	*90.85*	94.69
C(1)-O(1)	1.061(7)	1.163	*1.148*	1.150	C(2)-Re(1)-N(3)	96.2(2)	97.55	*98.18*	95.37
C(2)-O(2)	1.151(6)	1.158	*1.151*	1.147	C(3)-Re(1)-N(3)	173.2(2)	171.46	*176.35*	172.26
C(3)-O(3)	1.144(7)	1.159	*1.150*	1.154	N(2)-Re(1)-N(3)	74.94(16)	74.45	*76.24*	76.77
					C(1)-Re(1)-Cl(1)	176.98(17)	176.41	*174.84*	175.46
					C(2)-Re(1)-Cl(1)	91.93(19)	92.25	*91.51*	87.23
					C(3)-Re(1)-Cl(1)	92.71(19)	91.85	*90.34*	90.88
					N(2)-Re(1)-Cl(1)	82.80(12)	83.36	*86.05*	94.74
					N(3)-Re(1)-Cl(1)	85.64(13)	83.20	*88.34*	84.67
					Re(1)-C(1)-O(1)	176.0(6)	179.86	*179.21*	179.16
					Re(1)-C(2)-O(2)	177.4(5)	178.94	*179.89*	178.72
					Re(1)-C(3)-O(3)	177.6(6)	179.44	*178.55*	179.41

Table S5. Atomic charges from the Natural Population Analysis (NPA) for **ReL1** and **ReL2.**

Atom	Charge	
	ReL1	**ReL2**
Re(1)	–0.99	–1.00
C(1)	+0.74	+0.74
O(1)	–0.50	–0.50
C(2)	+0.78	+0.78
O(2)	–0.48	–0.48
C(3)	+0.76	+0.76
O(3)	–0.48	–0.48
N(2)	–0.39	–0.40
N(3)	–0.23	–0.18
Cl(1)	–0.46	–0.46

The calculated charge on Re(I) is slightly lower than the formal charge of +1 (which corresponds to a d^6 configuration of the central ion), as a result of charge donation from the N(2) and N(3) atoms of the ligand. The charge on the nitrogen atoms is significantly smaller and less negative, indicating higher electron density delocalization from the N(2) and N(3) atoms to Re(I) atom. The positively charged carbon atoms of the carbonyl ligands are found to accept as much as ∼0.76 (e) from Re(I). atom. The nitrogen atoms N(2) and N(3) donate as much as ∼0.40 (e) to Re(I).

Table S6. Occupancy and hybridization of the calculated natural bond orbitals (NBOs) between the rhenium and the carbonyl ligands for **ReL1** and **ReL2**.

Bond (X – Y)	Occupancy	Hybridization of NBO	EDX%	EDY%
		ReL1		
Re(1)–C(1)	1.919 (0.102)	0.597 $(sp^{2.89}d^{3.15})_{Re}$ + 0.802 $(sp^{0.53})_C$	35.65	64.35
Re(1)–C(2)	1.966 (0.200)	0.621 $(sp^{0.63}d^{2.58})_{Re}$ + 0.784 $(sp^{0.53})_C$	38.56	61.44
Re(1)–C(3)	1.965 (0.206)	0.618 $(sp^{0.67}d^{2.55})_{Re}$ + 0.786 $(sp^{0.52})_C$	38.16	61.84
C(1)–O(1)	1.996 (0.024)	0.558 $(sp^{1.96})_C$ + 0.830 $(sp^{1.30})_O$	31.16	68.84
	1.997 (0.245)	0.488 $(p)_C$ + 0.873 $(p)_O$	23.80	76.20
	1.995 (0.210)	0.497 $(p)_C$ + 0.868 $(p)_O$	24.67	75.33
C(2)–O(2)	1.997 (0.025)	0.556 $(sp^{1.98})_C$ + 0.831 $(sp^{1.31})_O$	30.90	69.10
	1.996 (0.208)	0.492 $(p)_C$ + 0.871 $(p)_O$	24.16	75.84
	1.995 (0.183)	0.498 $(p)_C$ + 0.867 $(p)_O$	24.79	75.21
C(3)–O(3)	1.997 (0.016)	0.558 $(sp^{1.90})_C$ + 0.830 $(sp^{1.20})_O$	31.16	68.84
	1.996 (0.219)	0.491 $(p)_C$ + 0.871 $(p)_O$	24.06	75.94
	1.995 (0.194)	0.495 $(p)_C$ + 0.869 $(p)_O$	24.53	75.47
		ReL2		
Re(1)–C(1)	1.922 (0.112)	0.596 $(sp^{2.72}d^{3.01})_{Re}$ + 0.803 $(sp^{0.53})_C$	35.54	64.46
Re(1)–C(2)	1.961 (0.144)	0.611 $(sp^{0.63}d^{2.13})_{Re}$ + 0.792 $(sp^{0.53})_C$	37.35	62.65
Re(1)–C(3)	1.960 (0.171)	0.614 $(sp^{0.65}d^{2.23})_{Re}$ + 0.790 $(sp^{0.52})_C$	37.66	62.34
C(1)–O(1)	1.997 (0.020)	0.560 $(sp^{1.93})_C$ + 0.829 $(sp^{1.26})_O$	31.32	68.68
	1.997 (0.243)	0.492 $(p)_C$ + 0.871 $(p)_O$	24.16	75.84
	1.994 (0.210)	0.499 $(p)_C$ + 0.867 $(p)_O$	24.90	75.10
C(2)–O(2)	1.997 (0.026)	0.555 $(sp^{2.01})_C$ + 0.832 $(sp^{1.34})_O$	30.84	69.16
	1.996 (0.193)	0.497 $(p)_C$ + 0.868 $(p)_O$	24.70	75.30
	1.995 (0.172)	0.501 $(p)_C$ + 0.866 $(p)_O$	25.10	74.90
C(3)–O(3)	1.997 (0.017)	0.559 $(sp^{1.90})_C$ + 0.830 $(sp^{1.21})_O$	31.19	68.81
	1.996 (0.213)	0.494 $(p)_C$ + 0.870 $(p)_O$	24.38	75.62
	1.995 (0.187)	0.498 $(p)_C$ + 0.867 $(p)_O$	24.84	75.16

The analysis of the natural bond orbitals (NBOs) is performed to understand the nature of the Re–CO bond. For each carbonyl group, three orbitals were detected for the C–O bond. All the Re–C bond orbitals are polarized towards the carbon atom, and the C–O bond orbitals are polarized towards oxygen. Each oxygen atom of the carbonyl ligand possesses one lone pair (LP) orbital. The occupancies of the anti-bonding NBOs are given in round brackets. The resonance structure 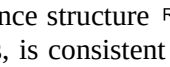 which presents the bond between Re atom and the CO ligand in complexes, is consistent with the calculated atomic charges.

Table S7. Natural populations of the $5d_{xy}$, $5d_{xz}$, $5d_{yz}$, $5d_{x^2-y^2}$ and $5d_{z^2}$ orbitals of the central atom in **ReL1** and **ReL2**.

Orbital	Natural population	
	ReL1	**ReL2**
d_{xy}	1.052	1.147
d_{xz}	1.364	1.520
d_{yz}	1.452	1.513
$d_{x^2-y^2}$	1.545	1.421
d_{z^2}	1.271	1.087

In free Re (I) state, the population of $5d_{xy}$, $5d_{xz}$ and $5d_{yz}$ orbitals are 2.0, 2.0 and 2.0 (e) and the other two ($5d_{x^2-y^2}$ and $5d_{z^2}$) orbitals remain vacant. In comparison, some decrease in populations for the $5d_{xy}$, $5d_{xz}$ and $5d_{yz}$ orbital and some increase in the populations of $5d_{x^2-y^2}$ and $5d_{z^2}$ orbital can be observed in both complexes.

Table S8. Absolute electronegativity, absolute hardness, dipole moment (μ), electrophilicity index (ω) and global softness (σ) of complexes **ReL1** and **ReL2** in CH_2Cl_2.

Parameters	**ReL1**	**ReL2**
E_{HOMO} (eV)	–6.60	–6.61
E_{LUMO} (eV)	–2.53	–2.23
Energy gap ΔE (eV)	4.07	4.38
Electronegativity μ (eV)	4.57	4.42
Hardness η (eV)	2.04	2.19
Dipole moment μ (Debye)	19.98	15.25
Electrophilicity ω (Debye/eV)	97.85	53.10
Softness σ (eV)	0.05	0.07

The frontier molecular orbital descriptors such as ionization potential (IP = $-E_{HOMO}$), electron affinity (EA = $-E_{LUMO}$), global hardness ($\eta = (I - A)/2$), electronegativity ($\chi = (I + A)/2$) chemical potential ($\mu = -\chi$), softness ($\sigma = 1/\eta$), global electrophilicity index ($\omega = \mu^2/2\eta$) were calculated according to Koopmans theorem (Koopmans, T. *Physica*, **1933**, *1*, 104-113).

Table S9. Energy levels and composition of selected frontier molecular orbitals for complexes **ReL1** and **ReL2** in CH_2Cl_2.

ReL1

	Orbital	Energy (eV)	MO Contribution (%)					Main bond type [a]
			Re	CO	Cl	Pyta	PBO	
123	LUMO+2	–1.63	0	1	0	95	4	π*(Pyta)
122	LUMO+1	–2.12	0	0	0	2	98	π*(PBO)
121	LUMO	–2.53	3	4	1	91	2	π*(Pyta)
			HOMO–LUMO gap (E = 4.07 eV)					
120	HOMO	–6.60	52	24	20	4	0	d(Re) + π(CO) + p(Cl)
119	HOMO–1	–6.71	52	22	22	5	0	d(Re) + π(CO) + p(Cl)
118	HOMO–2	–7.05	1	1	0	3	96	π(PBO)

ReL2

	Orbital	Energy (eV)	MO Contribution (%)					Main bond type [a]
			Re	CO	Cl	Pyta	PBO	
123	LUMO+2	–1.55	0	1	0	78	21	π*(Pyta) + π*(PBO)
122	LUMO+1	–2.16	1	2	0	25	73	π*(PBO) + π*(Pyta)
121	LUMO	–2.23	3	4	0	88	5	π*(Pyta)
			HOMO–LUMO gap (E = 4.38 eV)					
120	HOMO	–6.61	48	22	18	4	7	d(Re) + π(CO) + p(Cl)
119	HOMO–1	–6.71	47	20	20	4	8	d(Re) + π(CO) + p(Cl)
118	HOMO–2	–6.92	9	3	8	5	75	π(PBO)

[a] Pyta: pyridyltriazole, PBO: 2-phenylbenzoxazole

Table S10. The main electronic transitions for complex **ReL1** (in CH_2Cl_2), calculated with TDDFT method at the PBE1PBE/LANL2DZ level in comparison to the experimental values recorded in dichloromethane.

Electronic transition	Contribution	Assignment		E_{calc} /eV	λ_{calc} /nm	*f*	λ_{exp} /nm
$S_0 \rightarrow S_1$	HOMO → LUMO	d(Re) + π(CO) + p(Cl) → π*(Pyta)	MLCT/LLCT	3.07	403.9	*0.0010*	
$S_0 \rightarrow S_2$	H – 1 → LUMO	d(Re) + π(CO) + p(Cl) → π*(Pyta)	MLCT/LLCT	3.28	378.4	*0.1251*	384
$S_0 \rightarrow S_6$	HOMO → L + 2	d(Re) + π(CO) + p(Cl) → π*(Pyta)	MLCT/LLCT	4.12	300.9	*0.0568*	
	HOMO → L + 1	d(Re) + π(CO) + p(Cl) → π*(PBO)	MLCT/LLCT				
$S_0 \rightarrow S_8$	H – 2 → L + 1	π(PBO) → π*(PBO)	IL	4.24	292.8	*0.6072*	300
	H – 1 → L + 2	d(Re) + π(CO) + p(Cl) → π*(Pyta)	MLCT/LLCT				
$S_0 \rightarrow S_9$	H – 2 → L + 1	π(PBO) → π*(PBO)	IL	4.24	292.6	*0.5016*	
	H – 1 → L + 2	d(Re) + π(CO) + p(Cl) → π*(Pyta)	MLCT/LLCT				
$S_0 \rightarrow S_{12}$	H – 5 → LUMO	π(Pyta) + p(Cl) → π*(Pyta)	LLCT/IL	4.43	279.6	*0.1741*	272
$S_0 \rightarrow S_{25}$	H – 3 → L + 4	d(Re) + π(CO) → p(Re) + π*(CO)	MLCT/ILCT	5.08	244.2	*0.0446*	
	H – 3 → L + 6	d(Re) + π(CO) → p(Re) + π*(CO) + π*(PBO)	MLCT/LLCT/ILCT				
$S_0 \rightarrow S_{30}$	H – 5 → L + 2	π(Pyta) + p(Cl) → π*(Pyta)	LLCT/IL	5.34	232.1	*0.1156*	230

MLCT: metal-to-ligand charge transfer; LMCT: ligand-to-metal charge transfer; LLCT: ligand-to-ligand charge transfer; ILCT: intraligand charge transfer.

Table S11. The main electronic transitions for complex **ReL2** (in CH_2Cl_2), calculated with TDDFT method at the PBE1PBE/LANL2DZ level in comparison to the experimental values recorded in dichloromethane.

Electronic transition	Contribution	Assignment		E_{calc} /eV	λ_{calc} /nm	*f*	λ_{exp} /nm
$S_0 \rightarrow S_1$	HOMO → LUMO	d(Re) + π(CO) + p(Cl) → π*(Pyta)	MLCT/LLCT	3.39	365.3	*0.0040*	~350[a]
$S_0 \rightarrow S_2$	H – 1 → LUMO	d(Re) + π(CO) + p(Cl) → π*(Pyta)	MLCT/LLCT	3.57	347.4	*0.0801*	
$S_0 \rightarrow S_3$	HOMO → L + 1	d(Re) + π(CO) + p(Cl) → π*(PBO) + π*(Pyta)	MLCT/LLCT	3.82	324.4	*0.5028*	
$S_0 \rightarrow S_5$	H – 1 → L + 1	d(Re) + π(CO) + p(Cl) → π*(PBO) + π*(Pyta)	MLCT/LLCT	3.92	316.4	*0.3102*	
$S_0 \rightarrow S_6$	H – 2 → L + 1	π(PBO) → π*(PBO) + π*(Pyta)	ILCT/IL	4.08	304.1	*0.6416*	311
	H – 2 → LUMO	π(PBO) → π*(Pyta)	ILCT				
$S_0 \rightarrow S_7$	H – 2 → LUMO	π(PBO) → π*(Pyta)	ILCT	4.17	297.5	*0.0478*	
	H – 2 → L + 1	π(PBO) → π*(PBO) + π*(Pyta)	ILCT/IL				
$S_0 \rightarrow S_{17}$	H – 5 → LUMO	π(Pyta) + π(PBO) → π*(Pyta)	ILCT/IL	4.71	263.2	*0.1093*	278
$S_0 \rightarrow S_{18}$	H – 5 → L + 1	π(Pyta) + π(PBO) → π*(PBO) + π*(Pyta)	ILCT/IL	4.72	262.5	*0.0882*	
	H – 2 → L + 2	π(PBO) → π*(Pyta) + π*(PBO)	ILCT/IL				
$S_0 \rightarrow S_{27}$	H – 2 → L + 3	π(PBO) → π*(Pyta) + π*(PBO)	ILCT/IL	5.05	245.6	*0.0954*	
$S_0 \rightarrow S_{28}$	H – 3 → L + 4	d(Re) + π(CO) → p(Re) + π*(CO)	MLCT/ILCT	5.12	242.2	*0.1173*	
$S_0 \rightarrow S_{34}$	H – 4 → L + 2	π(PBO) → π*(Pyta) + π*(PBO)	ILCT/IL	5.43	228.5	*0.1500*	229
	HOMO → L + 5	d(Re) + π(CO) + p(Cl) → π*(PBO)	MLCT/LLCT				
$S_0 \rightarrow S_{36}$	H – 5 → L + 2	π(Pyta) + π(PBO) → π*(Pyta) + π*(PBO)	ILCT/IL	5.47	226.6	*0.0761*	

MLCT: metal-to-ligand charge transfer; LMCT: ligand-to-metal charge transfer; LLCT: ligand-to-ligand charge transfer; ILCT: intraligand charge transfer.
a: absorption tail.

Table S12. Four calculated lowest singlet excited states for complexes **ReL1** and **ReL2** in S_1 optimized geometry with TD-DFT method at the PBE1PBE/LANL2DZ level.

	State	Contribution	Assignment		E_{calc} (eV)	λ_{calc} (nm)	*f*
ReL1	1	HOMO → LUMO	d(Re) + π(CO) + p(Cl) → π*(pyta)	MLCT/LLCT	2.31	537.3	*0.0017*
	2	H – 1 → LUMO	d(Re) + π(CO) + p(Cl) → π*(pyta)	MLCT/LLCT	2.71	457.1	*0.1748*
	3	H – 2 → LUMO	d(Re) + π(CO) → π*(pyta)	MLCT/LLCT	3.00	413.5	*0.0022*
	4	HOMO → L + 1	d(Re) + π(CO) + p(Cl) → π*(PBO)	MLCT/LLCT	3.60	344.0	*0.0022*
ReL2	1	HOMO → LUMO	d(Re) + π(CO) + p(Cl) → π*(pyta)	MLCT/LLCT	2.67	463.6	*0.0018*
	2	H – 1 → LUMO	d(Re) + π(CO) + p(Cl) → π*(pyta)	MLCT/LLCT	3.01	411.0	*0.1242*
	3	H – 2 → LUMO	d(Re) + π(CO) + π(PBO) → π*(pyta)	MLCT/LLCT/ILCT	3.35	370.5	*0.0453*
		H – 3 → LUMO	d(Re) + π(CO) + π(PBO) → π*(pyta)	MLCT/LLCT/ILCT			
	4	HOMO → L + 1	d(Re) + π(CO) + p(Cl) → π*(PBO) + π*(pyta)	MLCT/LLCT	3.35	369.8	*0.1848*

MLCT: metal-to-ligand charge transfer; LMCT: ligand-to-metal charge transfer; LLCT: ligand-to-ligand charge transfer; ILCT: intraligand charge transfer.

Table S13. Calculated phosphorescence emission energies of **ReL1** and **ReL2**.

Compound	DFT		TD-DFT			
	ΔE_{T1}–S_0 (eV / nm)	Character	Major contribution (C_i coefficient)	E (eV)	λ_{cal} (nm)	Character
ReL1	2.03 / 610.8	^{3}MLCT/^{3}LLCT/^{3}IL	H → L (0.674)	1.92	645.1	^{3}MLCT/^{3}LLCT/^{3}IL
ReL2	2.38 / 520.9	^{3}MLCT/^{3}LLCT/^{3}IL	H → L (0.656)	2.24	553.2	^{3}MLCT/^{3}LLCT/^{3}IL

ΔE_{T1}–S_0 is the energy difference between the ground singlet and excited triplet states.

Table S14. Experimental electrochemical data used, and calculated values of the energy gaps (E_g) for compounds **ReL1** and **ReL2**.

Compound	$\mathbf{E_{onset}}$ **ox** (V)	$\mathbf{E_{onset}}$ **red** (V)	$\mathbf{E_{HOMO}}$ (eV)	$\mathbf{E_{LUMO}}$ (eV)	$\boldsymbol{E_g^{el}}$ (eV)	$\boldsymbol{E_{calc}}^*$ (eV)
ReL2	1.40	–1.45	–6.14	–3.29	2.85	3.01
ReL1	1.38	–1.17	–6.12	–3.57	2.55	2.71

* Values obtained from theoretical study, see Table 2.

Evaluation of the energy gap values (E_g) for the Re complexes.

The onset oxidation and reduction potentials (E_{onset} ox, E_{onset} red) were measured by cyclic voltammetry in volt *versus* SCE. The CVs were carried out at a potential scan rate of 200 mV s^{-1} at room temperature. The HOMO and LUMO energy levels (E_{HOMO} and E_{LUMO}) in electron volt (eV) were calculated according to the empirical equations (1) and (2):[1]

E_{HOMO} (eV) = -e (E_{onset} ox (V vs. SCE) + 4.74 V) *Eq(1)*

E_{LUMO} (eV) = -e (E_{onset} red (V vs. SCE) + 4.74 V) *Eq(2),*

and the energy gap value was obtained as follows: $E_g^{el} = (E_{LUMO} - E_{HOMO})$

The differences observed for the estimation of the energy gaps using experimental methods or theoretical calculations are well known. See for example: R. Stowasser, R. Hoffmann, *J. Am. Chem. Soc.* **1999**, *121*, 3414-3420.

[1] a) Y. Zhou, J. W. Kim, R. Nandhakumar, M. J. Kim, E. Cho, Y. S. Kim, Y. H. Jang, C. Lee, S. Han, K. M. Kim, J.-J. Kim, J. Yoon, *Chem. Commun.* **2010**, *46*, 6512-6514 and references therein; b) G. V. Loukova, *Chem. Phys. Lett.* **2002**, *353*, 244–252.

Table S15. Full spectroscopic data of the complexes in the three organic solvents. Maximum absorption wavelengths (λ_{abs}), molar extinction coefficients (ε), maximum fluorescence emission wavelengths (λ_F), fluorescence quantum yields (Φ_F), maximum phosphorescence emission wavelengths (λ_P), and phosphorescence quantum yields (Φ_P), luminescence decay times (τ_i) and their respective fractions of intensity (f_i). The decay times τ_i and the corresponding fractions of intensity f_i are defined by the multiexponential analysis of the decay curves: $I_F(t) = \Sigma a_i \times \exp(-t/\tau_i)$ and $f_i = a_i \times \tau_i / (\Sigma a_j \times \tau_j)$. If not specified, excitation was performed at 380 nm. The concentration of complexes was between to 2.0×10^{-5} M and 1.3×10^{-5} M for absorption, and between 1.3×10^{-5} M and 5×10^{-6} M for emission.

ReL1

	λ_{abs} (nm)	ε ($M^{-1}cm^{-1}$)	λ_P (nm)	Φ_P	τ_i (f_i)
Dichloromethane	296, 384	27800, 3900	628	0.017	1.69 ns (*0.03*), 74.7 ns (*0.97*) [a]
Acetonitrile	299, 364	34000, 4600	624	0.010	*nd*
Methanol	299, 362	*nd*	623	0.006	*nd*

ReL2

	λ_{abs} (nm)	ε ($M^{-1}cm^{-1}$)	λ_P (nm)	Φ_P	τ_i (f_i)
Dichloromethane	309	34100	546	0.015	4.79 ns (*0.04*), 192 ns (*0.96*) [b]
Acetonitrile	307	38600	542	0.006	*nd*
Methanol	307	*nd*	543	<0.002	*nd*

a: λ_{ex} = 330 nm, λ_{em} = 560-720 nm; *b*: λ_{em} = 500-630 nm.

Table S16. Results of the emission decay measurements of the complexes in the solid state. Emission wavelength (λ_{em}), luminescence decay times (τ_i) with their respective fractions of intensity (f_i). Excitation wavelength: 380 nm.

	λ_{em} (nm)	τ_1 (ns)	(f_1)	τ_2 (ns)	(f_2)	τ_3 (ns)	(f_3)	χ_R^2
ReL1	560-640	3.75	(0.07)	28.1	(0.03)	338	(0.90)	1.13
(solid)	610-690	3.75	(0.03)	28.1	(0.02)	338	(0.95)	1.06
ReL2								
(solid)	510-590	1.68	(<0.01)	41.4	(0.02)	414	(0.98)	1.16
	560-640	1.68	(<0.01)	41.4	(0.01)	414	(0.99)	1.16

Table S17. Cartesian coordinates of complex **ReL1**.

ReL1 in S_0

75	-0.377952000	-1.494063000	-1.404171000
7	6.234800000	-7.310917000	2.026945000
7	1.824218000	-1.618695000	-1.560897000
7	0.225439000	-3.043449000	-0.047830000
7	-0.460967000	-3.859339000	0.780248000
7	1.677103000	-4.407013000	0.815913000
8	-0.305940000	0.702967000	0.724493000
8	-3.407911000	-1.806970000	-1.018733000
8	-0.855536000	0.601319000	-3.603923000
8	4.976540000	-7.962088000	0.279868000
17	-0.298762000	-3.356629000	-3.105486000
6	-0.334109000	-0.133806000	-0.083692000
6	-2.267308000	-1.676075000	-1.170749000
6	-0.683082000	-0.185988000	-2.770071000
6	2.570790000	-0.832591000	-2.345126000
1	2.042922000	-0.063094000	-2.896067000
6	3.948474000	-0.978236000	-2.460546000
1	4.503247000	-0.312231000	-3.111636000
6	4.579746000	-1.981702000	-1.736178000
1	5.653070000	-2.125789000	-1.803608000
6	3.815704000	-2.806003000	-0.916372000
1	4.278727000	-3.595773000	-0.338021000
6	2.441647000	-2.597918000	-0.851944000
6	1.508615000	-3.360764000	-0.036351000
6	0.426105000	-4.674885000	1.292124000
1	0.225813000	-5.465445000	2.000492000
6	4.382274000	-6.863007000	0.812997000
6	3.225523000	-6.230004000	0.400598000
1	2.634556000	-6.559599000	-0.446735000
6	2.872300000	-5.117006000	1.163858000
6	3.617400000	-4.673749000	2.266967000
1	3.275139000	-3.802489000	2.816310000
6	4.777600000	-5.336836000	2.652064000
1	5.360380000	-5.002197000	3.503458000
6	5.159381000	-6.450972000	1.903424000
6	6.080594000	-8.168805000	1.061764000
6	6.932761000	-9.300323000	0.729797000
6	8.083513000	-9.535954000	1.495690000
1	8.318599000	-8.870632000	2.320401000
6	8.907441000	-10.613194000	1.193046000
1	9.798249000	-10.793606000	1.787249000
6	8.591319000	-11.460953000	0.129212000
1	9.236990000	-12.302500000	-0.104607000
6	7.446687000	-11.227920000	-0.633371000
1	7.199272000	-11.886397000	-1.460571000
6	6.616285000	-10.151347000	-0.337932000
1	5.725356000	-9.970083000	-0.930470000

ReL1 in S_1

75	-0.367149000	-1.504044000	-1.386370000
7	6.235284000	-7.312571000	2.031682000
7	1.768711000	-1.608609000	-1.627864000
7	0.201617000	-3.093344000	-0.140820000
7	-0.485487000	-3.954732000	0.655398000
7	1.673703000	-4.455009000	0.722241000
8	0.075584000	0.508379000	0.932587000
8	-3.428977000	-1.662906000	-0.934091000
8	-1.064210000	0.836262000	-3.309039000
8	4.994744000	-8.006132000	0.288701000
17	-0.487821000	-3.086822000	-3.213874000
6	-0.097573000	-0.237162000	0.077025000
6	-2.292655000	-1.603786000	-1.102406000
6	-0.789642000	-0.030795000	-2.604190000
6	2.520539000	-0.815462000	-2.419034000
1	1.979921000	-0.058084000	-2.977471000
6	3.885514000	-0.931382000	-2.541962000
1	4.424087000	-0.261736000	-3.201812000
6	4.554513000	-1.939997000	-1.793377000
1	5.630843000	-2.057439000	-1.864875000
6	3.822492000	-2.765271000	-0.978213000
1	4.308760000	-3.541364000	-0.398109000
6	2.417831000	-2.608199000	-0.888622000
6	1.524303000	-3.376979000	-0.116387000
6	0.404310000	-4.757520000	1.159598000
1	0.204307000	-5.570997000	1.841731000
6	4.391082000	-6.896696000	0.792995000
6	3.234962000	-6.276878000	0.357799000
1	2.653901000	-6.627051000	-0.488113000
6	2.865456000	-5.147560000	1.089749000
6	3.607085000	-4.678919000	2.186665000
1	3.257745000	-3.795081000	2.711171000
6	4.766632000	-5.327180000	2.597561000
1	5.342038000	-4.970371000	3.445185000
6	5.157607000	-6.458316000	1.879532000
6	6.092456000	-8.191271000	1.084153000
6	6.953329000	-9.325533000	0.782744000
6	8.086734000	-9.553506000	1.576246000
1	8.301871000	-8.881288000	2.400859000
6	8.919370000	-10.631558000	1.300935000
1	9.796354000	-10.805759000	1.917232000
6	8.630154000	-11.487563000	0.236070000
1	9.282957000	-12.329185000	0.023135000
6	7.503004000	-11.262091000	-0.554241000
1	7.276259000	-11.926521000	-1.382682000
6	6.663633000	-10.185309000	-0.285406000
1	5.786833000	-10.009416000	-0.900206000

ReL1 in T_1

75	-0.293299000	-1.625438000	-1.438336000
7	5.964044000	-7.550969000	2.304200000
7	1.834382000	-1.862585000	-1.763406000
7	0.270655000	-2.930874000	0.026140000
7	-0.403919000	-3.549654000	1.035705000
7	1.726393000	-4.204112000	1.075809000
8	0.186734000	0.779447000	0.457817000
8	-3.312246000	-1.717073000	-0.805800000
8	-0.937342000	0.396799000	-3.744836000
8	5.084541000	-7.645991000	0.236082000
17	-0.525026000	-3.407107000	-3.111245000
6	0.006054000	-0.115648000	-0.239996000
6	-2.185538000	-1.671359000	-1.046164000
6	-0.690019000	-0.346159000	-2.905238000
6	2.570033000	-1.261876000	-2.711988000
1	2.028551000	-0.612058000	-3.391902000
6	3.934902000	-1.432583000	-2.845938000
1	4.464225000	-0.920635000	-3.640914000
6	4.608369000	-2.273040000	-1.923276000
1	5.683703000	-2.407516000	-1.984946000
6	3.889475000	-2.912818000	-0.947381000
1	4.382552000	-3.554519000	-0.226829000
6	2.481921000	-2.726004000	-0.871677000
6	1.597608000	-3.304892000	0.044242000
6	0.466273000	-4.297406000	1.639304000
1	0.259153000	-4.946283000	2.478403000
6	4.393540000	-6.695713000	0.921107000
6	3.336368000	-5.924044000	0.481202000
1	2.918072000	-6.006650000	-0.516084000
6	2.833030000	-5.025258000	1.426054000
6	3.352783000	-4.929011000	2.727874000
1	2.921379000	-4.203201000	3.410261000
6	4.406689000	-5.736447000	3.142224000
1	4.808151000	-5.665027000	4.147471000
6	4.934641000	-6.631549000	2.211636000
6	6.007937000	-8.112690000	1.132613000
6	6.909778000	-9.161447000	0.680254000
6	7.868082000	-9.668589000	1.569623000
1	7.919734000	-9.270585000	2.578111000
6	8.737145000	-10.670198000	1.154317000
1	9.478058000	-11.060960000	1.845472000
6	8.658283000	-11.173053000	-0.146197000
1	9.338783000	-11.956148000	-0.467881000
6	7.705373000	-10.669950000	-1.032098000
1	7.641996000	-11.059669000	-2.043702000
6	6.831284000	-9.666798000	-0.624640000
1	6.089723000	-9.275409000	-1.313618000

Table S18. Cartesian coordinates of complex **ReL2**.

ReL2 in S_0

75	-7.392666000	-1.541419000	-5.588535000
7	0.703513000	-1.118441000	-0.786371000
7	-7.592278000	0.628001000	-5.965355000
7	-5.625622000	-0.644678000	-4.748268000
7	-4.606251000	-1.147139000	-4.124399000
7	-3.848795000	-0.112315000	-3.759407000
8	-6.091144000	-2.093228000	-8.303049000
8	-6.822091000	-4.423512000	-4.694526000
8	-10.128301000	-2.418110000	-6.681955000
8	-1.125259000	-2.376259000	-0.421756000
17	-8.394034000	-0.947872000	-3.351290000
6	-6.584362000	-1.882587000	-7.270717000
6	-7.046096000	-3.341113000	-5.040540000
6	-9.093449000	-2.092735000	-6.273081000
6	-8.624131000	1.198767000	-6.603636000
1	-9.382491000	0.527267000	-6.988891000
6	-8.733312000	2.572385000	-6.772260000
1	-9.590227000	2.979834000	-7.296534000
6	-7.735182000	3.394937000	-6.258123000
1	-7.791082000	4.472794000	-6.370947000
6	-6.661178000	2.814108000	-5.595930000
1	-5.864266000	3.421224000	-5.180585000
6	-6.620206000	1.428932000	-5.466630000
6	-5.545819000	0.712492000	-4.801566000
6	-4.384697000	1.066833000	-4.153642000
1	-3.933425000	2.019469000	-3.925482000
6	-1.438543000	-1.490904000	-1.403844000
6	-2.640059000	-1.343304000	-2.066861000
1	-3.514050000	-1.949826000	-1.861450000
6	-2.648036000	-0.331687000	-3.027299000
6	-1.532401000	0.474186000	-3.302792000
1	-1.592527000	1.223807000	-4.085058000
6	-0.344377000	0.303478000	-2.601827000
1	0.522480000	0.920866000	-2.810829000
6	-0.304778000	-0.701909000	-1.635559000
6	0.175043000	-2.090986000	-0.103767000
6	0.798939000	-2.890271000	0.939830000
6	2.129504000	-2.629694000	1.297766000
1	2.671272000	-1.838044000	0.789925000
6	2.738547000	-3.383073000	2.294081000
1	3.769079000	-3.179239000	2.569193000
6	2.028690000	-4.398055000	2.939286000
1	2.507475000	-4.984971000	3.717799000
6	0.705123000	-4.658623000	2.584055000
1	0.151611000	-5.447617000	3.084270000
6	0.087461000	-3.909353000	1.587483000
1	-0.942263000	-4.111499000	1.311029000

ReL2 in S_1

75	-7.401953000	-1.486451000	-5.510071000
7	0.703295000	-1.134608000	-0.791665000
7	-7.633658000	0.609853000	-5.918001000
7	-5.675069000	-0.620551000	-4.676494000
7	-4.649136000	-1.139873000	-4.033508000
7	-3.869799000	-0.115582000	-3.731573000
8	-5.986550000	-1.782202000	-8.254334000
8	-6.866309000	-4.425403000	-4.678850000
8	-10.024116000	-2.611803000	-6.738421000
8	-1.129179000	-2.380556000	-0.405446000
17	-8.548224000	-1.036858000	-3.425859000
6	-6.506205000	-1.681478000	-7.236015000
6	-7.066182000	-3.334477000	-4.986402000
6	-9.059707000	-2.178206000	-6.285999000
6	-8.672834000	1.196992000	-6.560716000
1	-9.461070000	0.528762000	-6.892682000
6	-8.763191000	2.546882000	-6.790211000
1	-9.629780000	2.944071000	-7.305944000
6	-7.709826000	3.398559000	-6.337680000
1	-7.751988000	4.469426000	-6.505396000
6	-6.642094000	2.832116000	-5.685131000
1	-5.820966000	3.445038000	-5.324329000
6	-6.595208000	1.440317000	-5.470390000
6	-5.556410000	0.750155000	-4.802234000
6	-4.360039000	1.071151000	-4.168006000
1	-3.869826000	2.009580000	-3.967582000
6	-1.446589000	-1.496785000	-1.388651000
6	-2.652820000	-1.345577000	-2.042025000
1	-3.528589000	-1.946180000	-1.827776000
6	-2.666328000	-0.337912000	-3.006990000
6	-1.547870000	0.461486000	-3.292757000
1	-1.611542000	1.208685000	-4.076795000
6	-0.354110000	0.286651000	-2.602973000
1	0.513756000	0.899261000	-2.821995000
6	-0.310379000	-0.715454000	-1.633349000
6	0.175597000	-2.101550000	-0.100668000
6	0.805283000	-2.900736000	0.939638000
6	2.141521000	-2.648075000	1.281932000
1	2.683125000	-1.862301000	0.764847000
6	2.756326000	-3.401472000	2.274694000
1	3.791246000	-3.203566000	2.537501000
6	2.046795000	-4.408804000	2.932118000
1	2.530143000	-4.995722000	3.707826000
6	0.717575000	-4.661480000	2.592623000
1	0.164093000	-5.444419000	3.102363000
6	0.094174000	-3.912077000	1.599681000
1	-0.940045000	-4.107911000	1.335653000

ReL2 in T_1

75	-7.802961000	-1.146490000	-4.945370000
7	0.140641000	-0.738116000	0.103324000
7	-7.475805000	0.501990000	-6.168854000
7	-5.927198000	-0.400582000	-4.266978000
7	-5.095316000	-0.795894000	-3.340414000
7	-4.106034000	0.087904000	-3.344189000
8	-6.588948000	-2.983018000	-7.126961000
8	-7.820933000	-3.622978000	-3.019402000
8	-10.640782000	-1.822065000	-5.941794000
8	-0.889314000	-2.527132000	-0.790059000
17	-8.734239000	0.158978000	-3.091310000
6	-7.030258000	-2.296149000	-6.317805000
6	-7.830531000	-2.718485000	-3.724978000
6	-9.575393000	-1.572879000	-5.574464000
6	-8.280449000	0.919147000	-7.204942000
1	-9.142413000	0.293681000	-7.408826000
6	-8.049025000	2.047137000	-7.931111000
1	-8.737093000	2.317659000	-8.724328000
6	-6.903769000	2.863766000	-7.632808000
1	-6.708141000	3.771872000	-8.192080000
6	-6.054798000	2.453464000	-6.625905000
1	-5.169732000	3.031952000	-6.376315000
6	-6.310648000	1.278788000	-5.911840000
6	-5.492097000	0.747413000	-4.880827000
6	-4.285830000	1.064193000	-4.268485000
1	-3.562041000	1.844170000	-4.439268000
6	-1.523549000	-1.422262000	-1.264791000
6	-2.587379000	-1.361186000	-2.142167000
1	-3.056655000	-2.237450000	-2.572838000
6	-3.014618000	-0.068178000	-2.445626000
6	-2.414539000	1.080714000	-1.906056000
1	-2.813276000	2.058680000	-2.154468000
6	-1.334899000	0.977520000	-1.036804000
1	-0.869681000	1.861974000	-0.615179000
6	-0.886604000	-0.303404000	-0.714209000
6	0.095787000	-2.034948000	0.023227000
6	0.959896000	-3.000107000	0.686270000
6	1.984786000	-2.538426000	1.524645000
1	2.115163000	-1.470140000	1.665793000
6	2.819499000	-3.447667000	2.163239000
1	3.612205000	-3.087034000	2.811971000
6	2.640213000	-4.819395000	1.971980000
1	3.294373000	-5.527479000	2.472501000
6	1.620827000	-5.280262000	1.138737000
1	1.479197000	-6.346456000	0.989166000
6	0.780441000	-4.376870000	0.495405000
1	-0.012750000	-4.735031000	-0.152851000

FIGURES

Crystallography

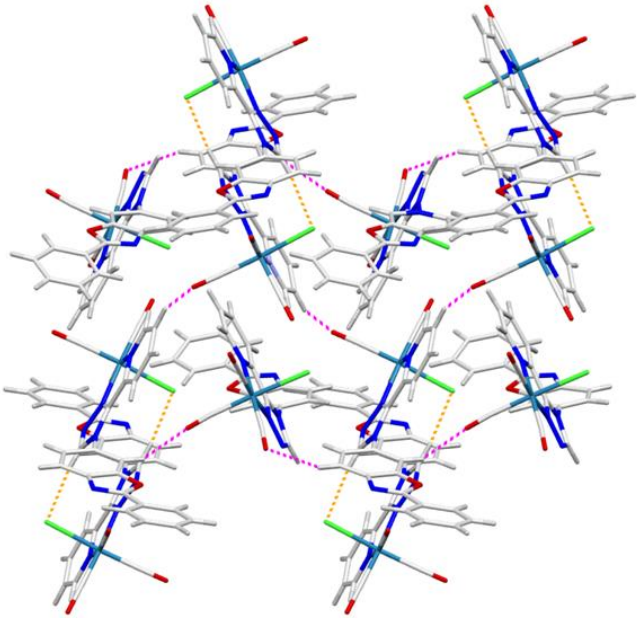

Intermolecular hydrogen bonding C—H···O interactions (magenta dash line) between C(12)-H donors and carbonyl oxygen O(5) acceptors, and between C(15)-H donors and carbonyl oxygen O(6) acceptors, as well as C—H···Cl interactions (orange dash line) between triazole C(10)-H donors and chloride Cl(1) acceptors in **ReL1**.

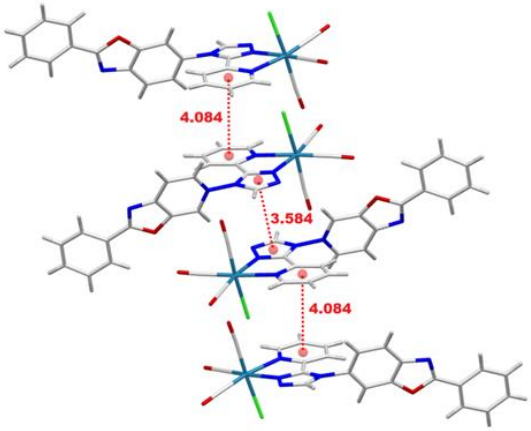

Intermolecular "pyridyl-pyridyl" and "triazolyl-triazolyl" distances between centroids in **ReL1**. Dashed lines link the centroids of two rings involved in each stacking interaction.

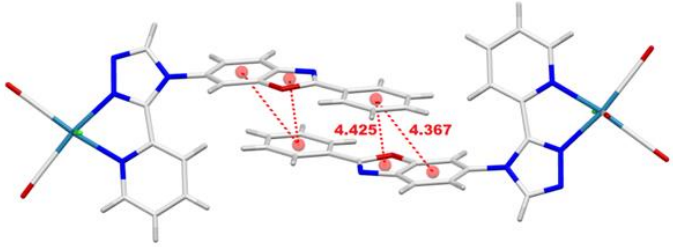

Intermolecular "benzyl-benzyl", "triazolyl-benzyl" distances between centroids in **ReL1**. Dashed lines link the centroids of two rings involved in each stacking interaction.

Figure S1. Hydrogen bonding and distances between centroids in **ReL1**.

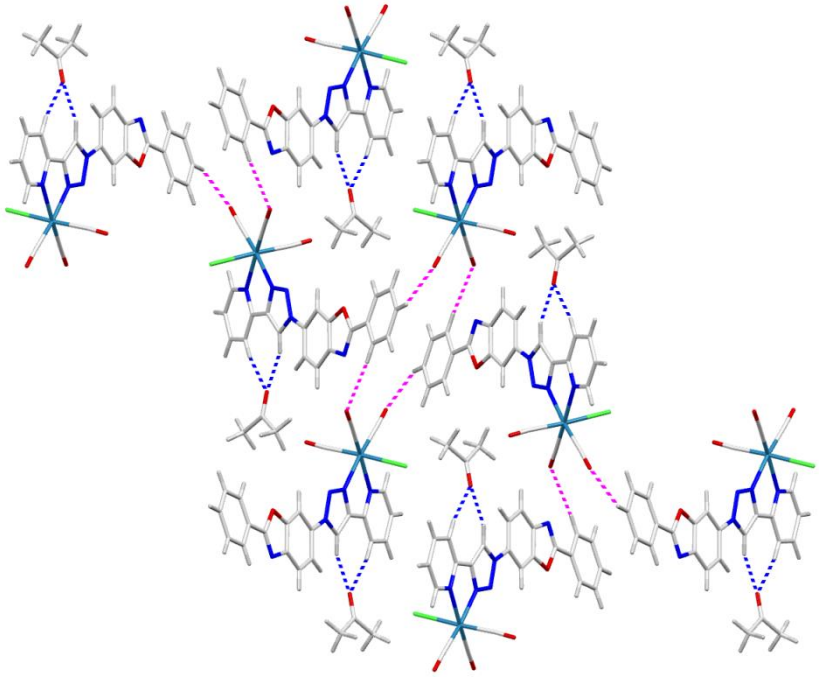

Intermolecular hydrogen bonding C—H···O interactions (magenta dash line) between C(19)–H and carbonyl oxygen O(3) and between C(21)–H and carbonyl oxygen O(2), as well as C—H···O interactions (blue dash line) between C(10)–H proton of the triazole or 5-C(7)–H proton of the 2-pyridyl group and the oxygen atom O(5) of acetone molecule in **ReL2**.

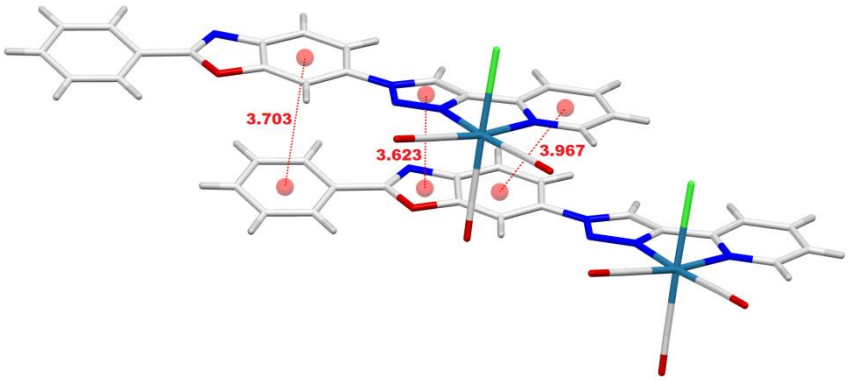

Intermolecular "benzyl-benzyl", "triazolyl-oxazolyl" or "pyridyl-benzyl" π,π-stacking interactions in **ReL2**. Dashed lines link the centroids of two rings involved in each stacking interaction.

Figure S2. Hydrogen bonding and distances between centroids in **ReL2**.

Results of DFT calculations

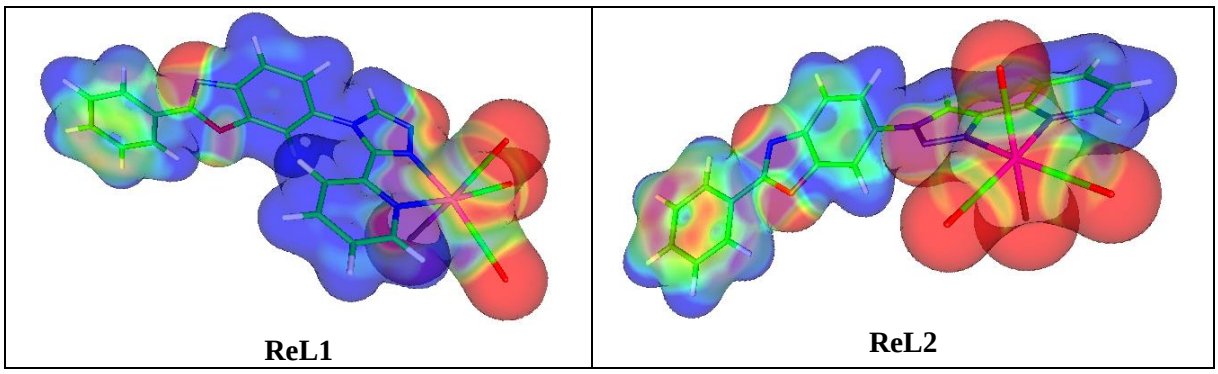

Figure S3. Molecular electrostatic potential (MEP) surface of **ReL1** and **ReL2.**
The electrostatic potential is mapped onto the total electron density.

In the MEP surface map, regions are represented by different colors which corresponds to different values of the electrostatic potential. The maximum negative region which preferred site for electrophilic attack is indicated as red color, whereas the maximum positive region which preferred site for nucleophilic attack is indicated as blue color. Potential increases in the order red < orange < yellow < green < cyan < blue, where red shows the strongest repulsion and blue shows the strongest attraction. Regions having the negative potential are over the electronegative atoms while the regions having the positive potential are over the electropositive atoms.

In Figure S3, the negative electrostatic potential regions (red colour) of complexes **ReL1** and **ReL2** are mainly localized around the oxygen O(4) and the nitrogen N(1) of the benzoxazole, the nitrogen N(2) of the pyridine ring, the nitrogens N(3) and N(4) of the triazole ring, chlorine Cl(1) as well as carbonyl oxygens O(1), O(2), O(3). The positive electrostatic potential regions (blue colour) are around the hydrogen atoms.

Electrochemical selected curves

OSWV study was performed on a Pt working electrode in CH_2Cl_2 + 0.1 M *n*[Bu_4N][BF_4] at room temperature in the presence of ferrocene used as internal reference. Frequency 20 Hz, amplitude 20 mV, step potential 5 mV.

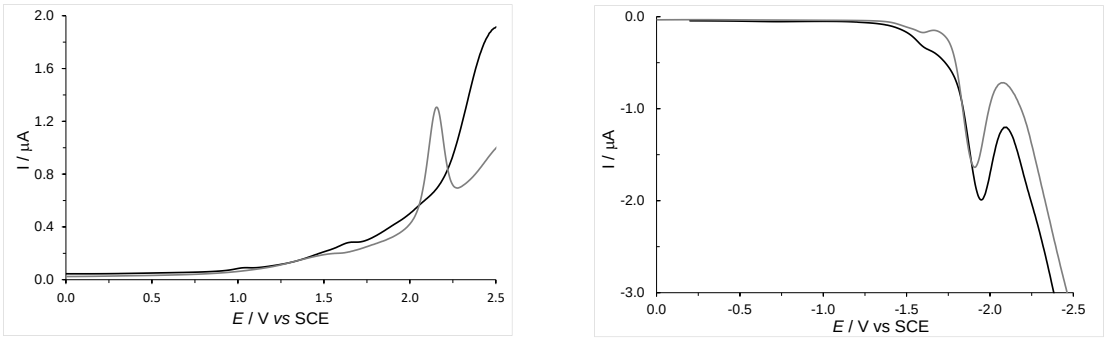

Figure S4. Anodic (left) and cathodic (right) scans of ligand **L1** (black) and **L2** (grey).

Cyclic voltammograms of the indicated compounds on a Pt working electrode in CH_2Cl_2 + 0.1 M *n*[Bu_4N][BF_4] at room temperature at a scan rate of 200 mVs^{-1} toward cathodic potentials.

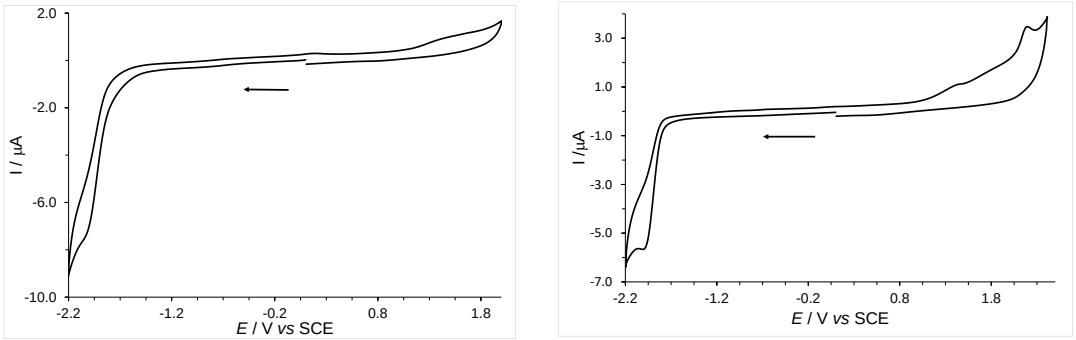

Figure S5. Cyclic voltammograms of ligands **L1** (left) and **L2** (right).

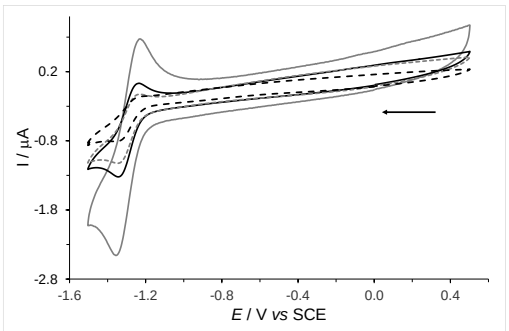

Figure S6. First reduction process of complex **ReL1** at respectively, 0.2 (dashed black), 0.5 (dashed grey), 1.0 (black), and 5.0 (grey) V/s.

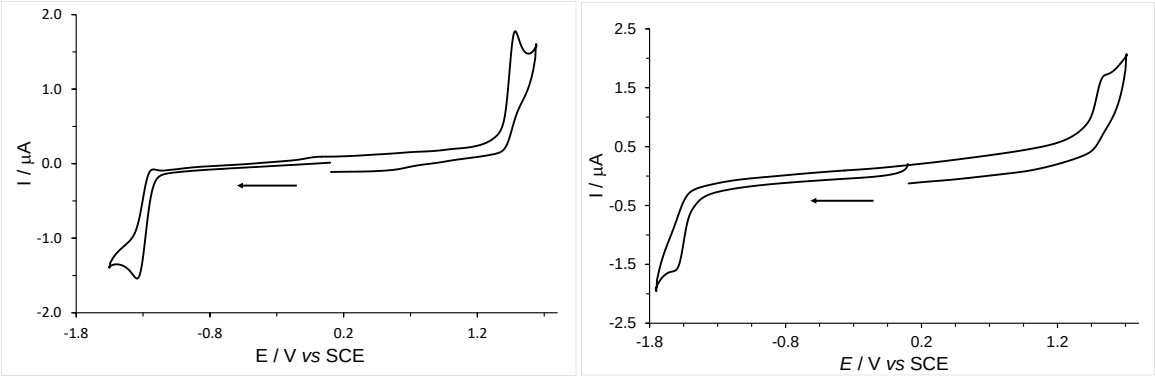

Figure S7. Cyclic voltammograms of complexes **ReL1** (left) and **ReL2** (right).

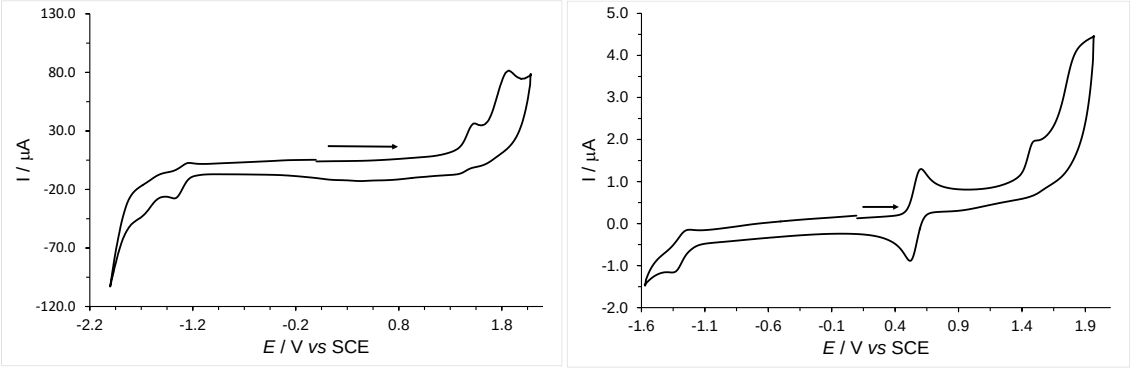

Figure S8. Cyclic voltammograms of complex **ReL1** on a glassy carbon working electrode (left), and after ferrocene addition (right) on a Pt working electrode.

Spectroscopy

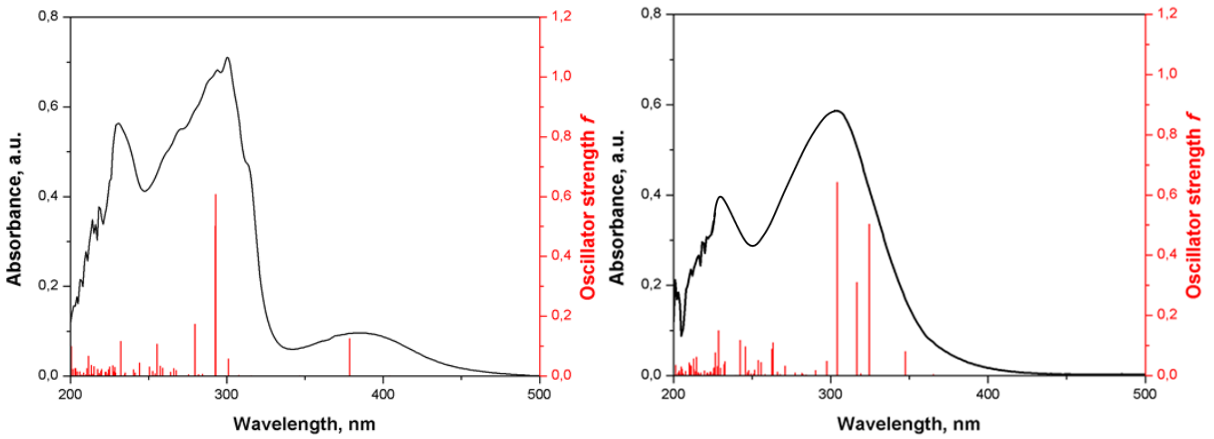

Figure S9. Comparison between the experimental (black) and simulated (red) UV-vis absorption spectra of complex **ReL1** (left) and **ReL2** (right) in CH_2Cl_2.

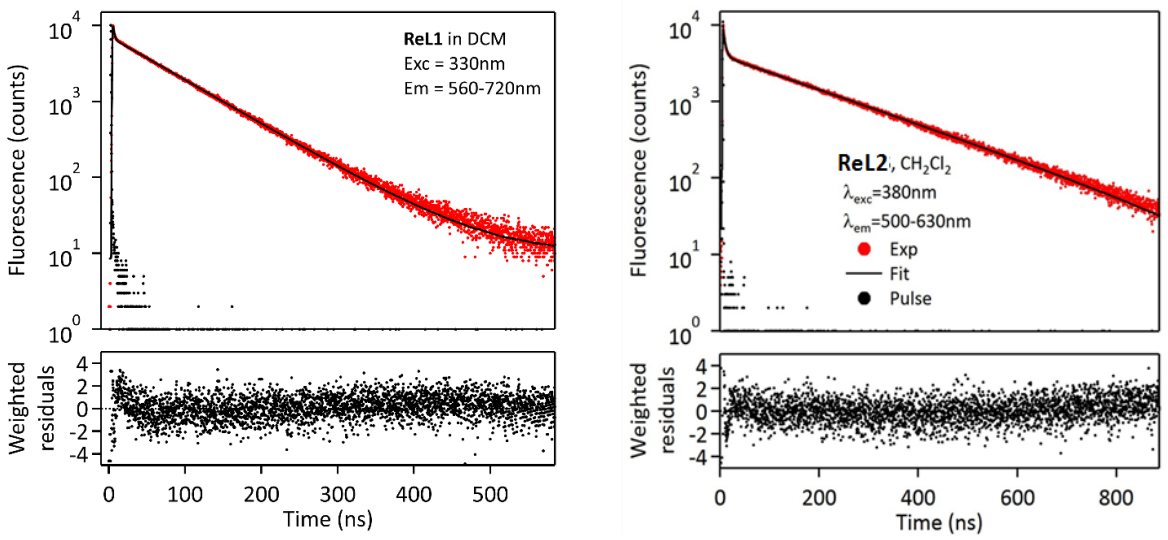

Figure S10. Fluorescence decays of complexes **ReL1** (left) and **ReL2** (right) in dichloromethane. For **ReL1**, the decay was analyzed with two time constants: the short one τ_1 = 1.69 (f_1 = 0.03) ns is attributed to a fluorescent impurity, whereas the long decay τ_2 = 74.7 ns (f_2 = 0.97) represents the main part of the red emission.

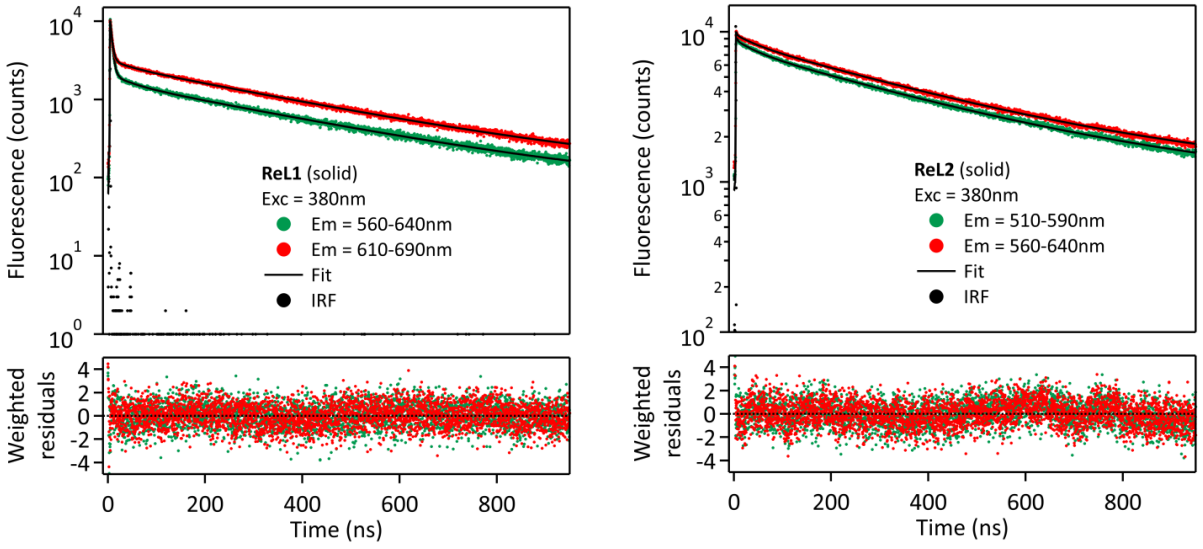

Figure S11. Fluorescence decays of complexes **ReL1** (left) and **ReL2** (right) in the solid state (powder).

Proton numbering scheme

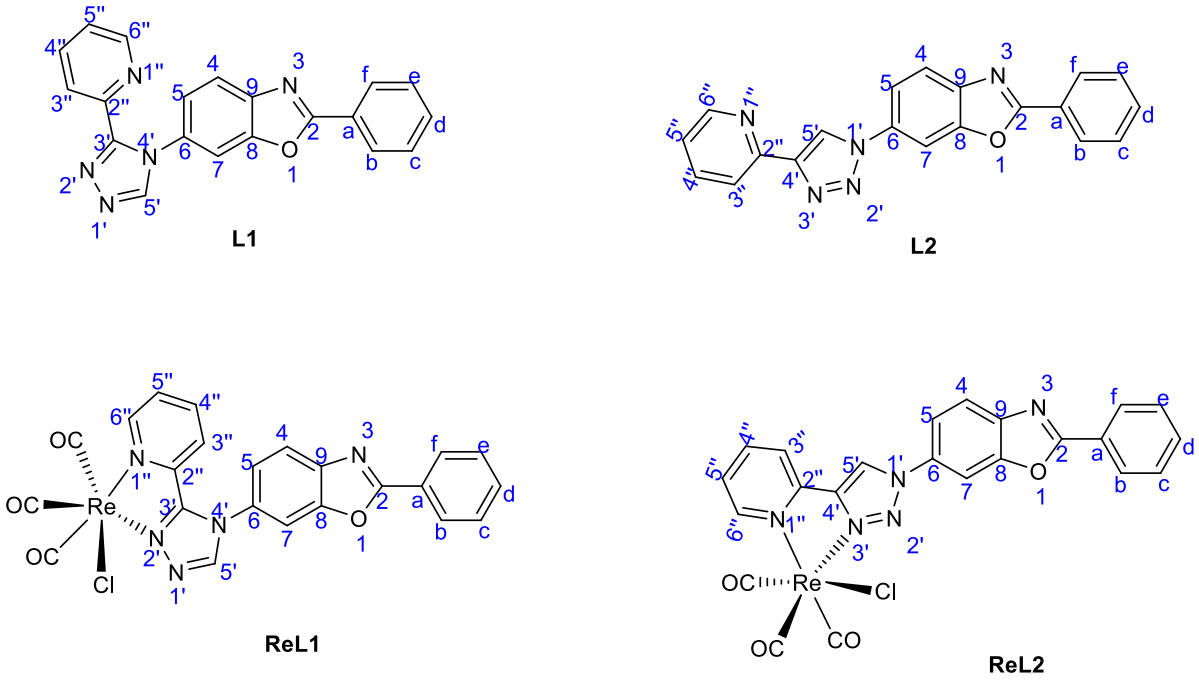

Figure S12. Proton numbering scheme for NMR.